Stabilization of electrically conducting capillary bridges using feedback control of radial electrostatic stresses and the shapes of extended bridges

Mark J. Marr-Lyon, David B. Thiessen, Florian J. Blonigen, and Philip L. Marston

Citation: Physics of Fluids **12**, 986 (2000); doi: 10.1063/1.870354
View online: https://doi.org/10.1063/1.870354
View Table of Contents: http://aip.scitation.org/toc/phf/12/5
Published by the American Institute of Physics

Stabilization of electrically conducting capillary bridges using feedback control of radial electrostatic stresses and the shapes of extended bridges

Mark J. Marr-Lyon, David B. Thiessen, Florian J. Blonigen, and Philip L. Marston
Department of Physics, Washington State University, Pullman, Washington 99164-2814

(Received 28 October 1999; accepted 12 January 2000)

Electrically conducting, cylindrical liquid bridges in a density-matched, electrically insulating bath were stabilized beyond the Rayleigh–Plateau (RP) limit using electrostatic stresses applied by concentric ring electrodes. A circular liquid cylinder of length L and radius R in real or simulated zero gravity becomes unstable when the slenderness $S=L/2R$ exceeds π. The initial instability involves the growth of the so-called (2, 0) mode of the bridge in which one side becomes thin and the other side rotund. A mode-sensing optical system detects the growth of the (2, 0) mode and an analog feedback system applies the appropriate voltages to a pair of concentric ring electrodes positioned near the ends of the bridge in order to counter the growth of the (2, 0) mode and prevent breakup of the bridge. The conducting bridge is formed between metal disks which are grounded. Three feedback algorithms were tested and each found capable of stabilizing a bridge well beyond the RP limit. All three algorithms stabilized bridges having S as great as 4.3 and the extended bridges broke immediately when feedback was terminated. One algorithm was suitable for stabilization approaching $S=4.493...$ where the (3, 0) mode is predicted to become unstable for cylindrical bridges. For that algorithm the equilibrium shapes of bridges that were slightly under or over inflated corresponded to solutions of the Young–Laplace equation with negligible electrostatic stresses. The electrical conductivity of the bridge liquid need not be large. The conductivity was associated with salt added to the aqueous bridge liquid.
[S1070-6631(00)00505-5]

I. INTRODUCTION

The stability of a weightless column of liquid between identical circular supports is ordinarily governed by capillary forces. When the volume of the liquid column is constrained to be that of a circular cylinder between coaxial supports, the column first becomes unstable when its length L exceeds $2\pi R$ where R is the radius of the supports.[1–5] In the discussion which follows, this condition is referred to as the Rayleigh–Plateau (RP) limit and the corresponding limit for the slenderness $S=L/2R$ is π. In this paper a novel method for suppressing the RP instability is demonstrated based on the active control of electrostatic stresses on a grounded liquid bridge. While the experimental demonstration was limited to situations in which the electrical conductivity of the bridge was enhanced by adding salt (NaCl) to the bridge liquid, it is anticipated that a similar method may be useful for certain situations in which the electrical conductivity of the liquid is small. In the experiments, the weightless condition is established by the Plateau tank method where, for the present application, the electrical conductivity is negligible for the outer (density matched) liquid. The electric field and associated stresses are nearly radial since the bridge is grounded.

The present study differs in various aspects with prior investigations of methods for suppressing the RP instability. Electric-field based methods have emphasized liquids which are good insulators and passive electric fields which are applied axially.[6] Axisymmetric laminar flow has been shown to influence the RP instability.[7] Of the various methods for stabilization which have been previously investigated, the active control[8] of acoustic radiation stresses[9] has the greatest similarity with the approach considered here.

Some situations where the RP instability is relevant include the following: materials processing based on the floating zone method,[3,10,11] drop formation and the breakup of laminar liquid jets,[12,13] the coating of solid fibers,[14] and the release of air bubbles from an underwater nozzle.[15] It is noteworthy that the boundary conditions of fixed circular contact curves of equal radius may be insufficient for describing floating zone crystallization even in low gravity,[16,17] and for that application the liquid volume might not be constrained to be at (or near) $\pi R^2 L$ as in our experiments. Nevertheless, feedback control strategies for suppressing capillary driven instabilities are relevant.

II. ACTIVE STABILIZATION USING ELECTRIC FIELDS

As was previously demonstrated,[8] the slenderness of a liquid bridge in a Plateau tank may be extended significantly beyond the RP limit by optically sensing the amplitude and phase of the axisymmetric mode of interest and using the information to rapidly control the spatial distribution of the acoustic radiation stress. The first mode which naturally becomes unstable for a circular cylindrical bridge of fixed volume having pinned contact circles at the ends is denoted here by $(n,m)=(2,0)$, where n is an axial index and m is an azimuthal index. This mode displays a left–right (L–R)

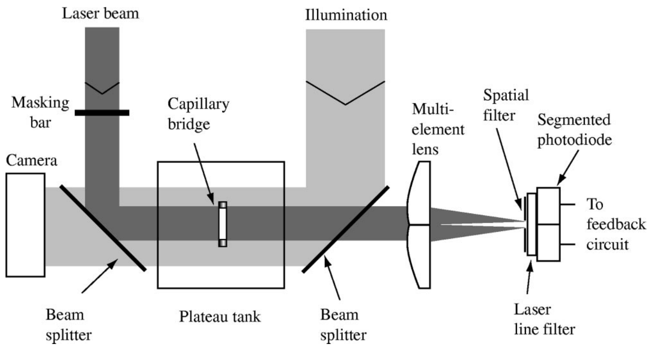

FIG. 1. The bridge is illuminated with an expanded laser beam, which is focused onto the segmented photodiode by a two-element lens that projects half of the bridge on each photodiode segment. The difference in signal between the two segments is then a measure of the (2, 0) mode deformation. The bridge is horizontal in the Plateau tank and this is the top view.

asymmetry when viewed from the side as shown, e.g., in Fig. 2(b) of Morse *et al.*,[9] where a similar notation is used. Additionally, all other axisymmetric modes of a cylindrical bridge (n, 0) for $n=3,4,...$ also become unstable if S is sufficiently large. The slenderness S_n at which the (n, 0) mode, where $n=2,3,...$, becomes unstable, is given by the $(n/2)$th lowest nonzero root of $\tan S=0$ if n is even, and by the $[(n-1)/2]$th lowest nonzero root of $\tan S=S$ if n is odd.[18,19] For the two modes of interest—the (2, 0) and (3, 0) modes—S_2 is simply the RP limit of π, and $S_3\approx 4.49341$. The stability limit of the (3, 0) mode is of interest since the stabilization methods described herein are applied only to the (2, 0) mode instability, thus the bridge stabilized by these methods will break when the (3, 0) mode becomes unstable. This limit will be discussed further in Sec. IV.

A. Stabilization methods

In the present work (as well as in Marr-Lyon *et al.*[8]), an error voltage V_e is optically generated which is proportional to the L–R asymmetry of the bridge. This signal is generated by illuminating the bridge with a laser beam and by detecting the light which passes by the bridge without being scattered by the bridge using a photodiode having two segments as shown in Fig. 1. An additional description of the apparatus is given in Sec. III. The principle of operation is that if the left side of the bridge becomes rotund and the right side thins, the optical power detected by the photodiode on the left decreases while the power into the right diode increases and this imbalance is used (with the aid of a differential amplifier) to produce the error voltage V_e which may be either positive or negative depending on which end of the bridge is rotund.

The error voltage is processed and used to adjust the potentials of a pair of ring electrodes which are concentric with the axis of the cylinder. Let V_L and V_R denote the potentials of the electrodes closest to the left and right ends of the cylinder, respectively. The circular metal disks on each end of the bridge are held at ground potential. The electrical conductivity of the bridge liquid is taken to be sufficiently large that the bridge liquid (to a good approximation) is maintained at ground potential. The experiment is carried out in a Plateau tank in which the outer bath liquid is a good insulator with a dielectric constant that is not large. As a consequence, it may be shown (see the Appendix) that the electrical conductivity of the bridge liquid is not required to be large and it was sufficient to add 2% by weight of salt to a mixture of water and methyl alcohol. The lower limit of salt concentration was not determined experimentally. As explained in the Appendix, the dimensions of the electrodes were selected in such a way that the electric-field distribution outside the surface of the bridge was appropriate for applying a stress to the side of the bridge closest to the electrode without significantly applying a stress to the other side of the bridge. For the situation where the bridge liquid is maintained at ground potential, the electrostatic stress is radially outward and in the region closest to the left (right) electrode is proportional to $V_L^2(V_R^2)$. The electric field in the portion of the bridge near either electrode is only weakly affected by the electrode potential on the opposite end. Stabilization of the liquid bridge to a slenderness significantly beyond the natural limit of π was achieved by using three different algorithms for adjusting the electrode voltages V_L and V_R. For definiteness in the discussion which follows, let positive values of the error voltage V_e correspond to the situation where the left side of the bridge is slender and the right side of the bridge is rotund. In the simplified discussion of the control method described below, the finite frequency response of the control system is neglected so that any delays in adjusting the potentials V_L and V_R are omitted from consideration. The three methods for selecting the electrode potentials are summarized as follows.

1. Method 1: Simple feedback

The potential of the electrode adjacent to the slender side of the bridge is raised in proportion to V_e while the opposite electrode remains at ground potential,

$$V_L=KV_e, \quad V_R=0 \quad (V_e\geqslant 0), \tag{1a}$$

$$V_L=0, \quad V_R=KV_e \quad (V_e<0), \tag{1b}$$

where K is a positive gain constant incorporating the gain of a high-voltage amplifier. This method has the property that the difference in the stresses applied to the left and right side of the bridge has a magnitude proportional to V_e^2, which introduces certain complications as explained in Sec. IV.

2. Method 2: Square-root feedback

The simplest method to generate a stress difference which varies in magnitude proportional to $|V_e|$ is to use a circuit which takes the square root of $|V_e|$ prior to amplification. As in method 1, the potential of the opposite electrode remains at ground potential,

$$V_L=K|V_e|^{1/2}, \quad V_R=0 \quad (V_e\geqslant 0), \tag{2a}$$

$$V_L=0, \quad V_R=-K|V_e|^{1/2} \quad (V_e<0), \tag{2b}$$

where K is a positive gain constant as in Eq. (1).

3. Method 3: Bias potential feedback

Another method in which the generalized force for the mode of interest is linear in the error signal V_e is to introduce a bias voltage and to consider the difference between the stresses on the left and right sides of the bridge. The electrode voltages are taken to be

$$V_L = V_b + KV_e, \quad V_R = -V_b + KV_e, \tag{3}$$

for all V_e where V_b is a bias voltage. It follows that the generalized force for the mode of interest is proportional to

$$V_L^2 - V_R^2 = 4KV_bV_e, \tag{4}$$

which is linear in V_e. The effective gain of the system is now proportional to the bias voltage V_b. As explained in Sec. IV, this method has the complication that for a symmetric bridge giving $V_e = 0$, each electrode has a potential of magnitude V_b so that there is a radially outward stress on each end of the bridge.

B. Feedback delay time

In the analysis presented in the Appendix to Marr-Lyon *et al.*,[8] one of the requirements for feedback control to stabilize the bridge is that the generalized force F_{feedback} for the mode of interest must not lag significantly behind the modal amplitude detected by the optical sensor. In practice, some delay is necessary because the frequency response of the amplifier circuitry is diminished at high frequencies. The simplest causal approximation of the impulse response of the control circuitry is the one-sided exponential $h(t) = H(t)e^{-t/\tau}$, where τ is a time constant and $H(t)$ is a step function which vanishes for $t<0$. For control methods 2 and 3, F_{feedback} is proportional to the convolution of the error voltage $V_e(t)$ with $h(t)$. The characteristic equation of the bridge mode with feedback follows from the analysis in Marr-Lyon *et al.*, as will now be demonstrated. Let $x(t) = x_0 e^{i\Omega t}$ denote the amplitude of the (2, 0) bridge mode where Ω is a complex frequency and V_e is proportional to the (real part of) $x(t)$. Assuming that $|\Omega\tau| \ll 1$, from the convolution with $h(t)$, the feedback force becomes

$$F_{\text{feedback}} \approx -Gx_0 e^{-i\Omega\tau} e^{i\Omega t}, \tag{5}$$

where G is a gain constant. The force in Eq. (5) is of the form considered by Marr-Lyon *et al.* The characteristic equation for the natural frequency Ω of the controlled mode is reducible to[8]

$$\omega_n^2 - \Omega^2 + \alpha_n i(1+i)\Omega^{3/2} + i\gamma_n\Omega = 0, \tag{6}$$

where α_n and γ_n are normalized modal damping constants which depend on the viscosities of the inner and outer liquids and ω_n^2 is a normalized effective spring constant for the mode. For the bridge to be stable, it is necessary to have both $\omega_n^2 > 0$ and $\gamma_n > 0$. (The damping parameter α_n is positive and is only weakly affected by the choice for τ.) The variation of ω_n and γ_n with τ is such that for stability the gain G must be in the range[8]

$$-k < G < \gamma_e m_b/\tau, \tag{7}$$

where $k = m_b\omega_b^2$ and m_b are the effective spring constant and "bare" mass for the (2, 0) mode of the corresponding inviscid system[18] and γ_e is an effective damping constant in the absence of feedback. For bridges longer than $S=\pi$, k becomes negative[8] so the gain must be positive but not larger than $\gamma_e m_b/\tau$. The result that the maximum allowable gain is proportional to $1/\tau$ agrees with standard control theory.[20] As S is increased significantly beyond π, k becomes increasingly negative and it becomes impossible to control the (2, 0) mode if $-k$ exceeds $\gamma_e m_b/\tau$ and (as assumed here) the controller uses only displacement information. Our results presented in Sec. IV indicate that for the bridge system used in these experiments, this crossover does not occur prior to the onset of (3, 0) mode instability. For control method 1 the feedback force is nonlinear in x and this model is not directly applicable.

III. DESCRIPTION OF EXPERIMENTAL APPARATUS

A. Plateau tank

A horizontal liquid cylinder consisting of a mixture of 62.0 wt% water, 36.0 wt% methanol, and 2.0 wt% salt (NaCl) is formed between two 0.432 cm diameter stainless-steel disks in a density-matched bath of 20 cS silicone oil (Dow Corning 200 fluid, $\rho = 0.951\ \text{g/cm}^3$). The salt provides significantly more than the minimum conductivity required, as explained in the Appendix. Two ring electrodes which are concentric with the bridge are spaced by 1.16 cm. The rings are 1.23 cm in diameter and are made of 0.12 cm diameter copper wire. The ring diameter was chosen to give optimal coupling of the electrostatic stress profile to the (2, 0) mode of the bridge, as explained in the Appendix. The voltages on the ring electrodes are varied as needed in order to stabilize a liquid bridge while the disks are held at ground potential.

An automated system injects the bridge liquid through a hole in one of the end disks and simultaneously retracts the disks at such a rate that the liquid bridge remains cylindrical during extension. The disk separation and bridge volume may also be adjusted independently.

B. Optics

The deformation of the bridge is detected optically, as shown in Fig. 1. The beam of a semiconductor laser is expanded and illuminates the bridge, and a two-element lens focuses the laser beam passing by each half of the bridge onto a separate photodiode element. A spatial filter placed at the focal plane of the lenses prevents light scattered by the bridge from entering the photodiode. The photodiode is positioned as close to the focal plane of the lenses as possible so all of the light collected by the lenses falls on the appropriate segment of the photodiode. This method allows for increased sensitivity and easier alignment than the previously described method using a single lens.[8]

The two-element lens is composed of two circular plano-convex lenses of focal length f modified as shown in Fig. 2. Both lenses are cut along a chord such that the lens centers are separated by a distance d, determined by the size and configuration of the photodiode elements. The radius r of the

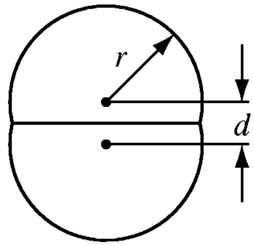

FIG. 2. Front view of the dual-lens system.

lenses must be large enough so that vignetting of the bridge by the lenses does not occur, and f must be long enough so that all of the parallel rays entering the lens fall on the photodiode element, which is positioned behind the focal plane of the lenses. In the system used for stabilization, the parameters are as follows: $f=175$, $d=6$, $r=12.5$ mm, and the photodiode is approximately 20 mm behind the focal plane of the lenses.

Since the expanded semiconductor laser beam is not spatially uniform, a horizontal masking bar is placed in the beam path at the same height as the bridge (see Fig. 1). The bar has a diameter slightly less than that of the end disks, but greater than that of the supporting rods. This results in a much decreased sensitivity of the optical signal difference to the bridge length.

C. Feedback algorithms

As described in Sec. II, three feedback methods were used for stabilization. The general form of the implementation of all three methods is outlined in Fig. 3. The photodiode signals are amplified, and the difference is taken. An adjustable offset voltage V_o is then added to the difference signal to compensate for laser beam irregularities and other optical imperfections, giving the error signal V_e. The error signal is input to the feedback circuit which generates a single output voltage V_f that is then input to a high voltage amplifier. The output of the amplifier V_a is then input to a high-voltage circuit which produces two output voltages V_R and V_L on the electrodes.

The high-voltage amplifier (Trek model 677B) has a maximum output voltage of ± 2 kV and a maximum slew rate of 15 V/μs, and has an adjustable current limit in the range 0–5 mA to avoid catastrophic failure when the bridge breaks and shorts an electrode to ground. All circuits in the feedback loop use analog components to keep the delay time τ as small as possible, though in principle a fast digital system could also be used. From the frequency response of the Trek amplifier a lower limit for τ is estimated to be 0.03 ms.

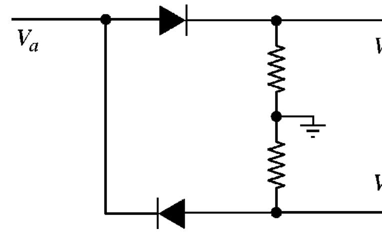

FIG. 4. High-voltage circuit using diodes.

1. Method 1: Simple feedback

The simplest feedback algorithm is $V_f=K_1V_e$, where K_1 is an adjustable positive gain constant. Using rectifiers as shown in Fig. 4, the high-voltage output V_a is split such that V_L and V_R are given by Eq. (1). As previously noted in Sec. II, the net force on the bridge is proportional to the square of the electrode potential, so this linear feedback algorithm results in a nonlinear feedback force.

2. Method 2: Square-root feedback

In this method, $V_f=K_2V_e|V_e|^{-1/2}$, where K_2 is again an adjustable positive gain constant. Using the high-voltage circuit in Fig. 4, the electrode potentials are given by Eq. (2). Calculation of the square-root is accomplished using logarithmic amplifiers, and therefore the circuit does not behave ideally near $V_e=0$. However, this had no observable effect on the stabilized bridge.

3. Method 3: Bias potential feedback

In this method, a bias potential is introduced into the high-voltage circuit as in Fig. 5 such that $V_L=V_a+V_b$ and $V_R=V_a-V_b$. The linear feedback algorithm $V_f=K_1V_e$ of method 1 is used to produce the electrode potentials given by Eq. (3).

IV. RESULTS AND DISCUSSION

As discussed in previous sections, bridge stabilization is accomplished by sensing when the bridge is becoming deformed with a L–R asymmetry and then applying voltages to the ring electrodes to counter the growth of the deformation. The three different algorithms for determining the electrode potentials which were discussed previously were each tested and found capable of stabilizing a bridge well beyond the RP

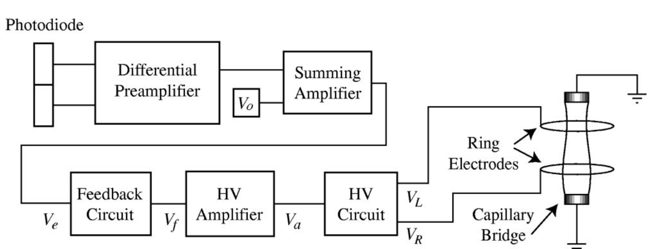

FIG. 3. Feedback block diagram.

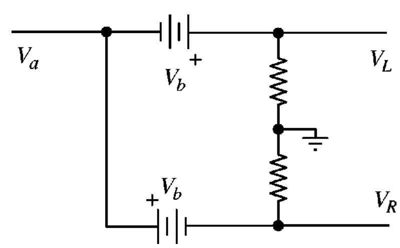

FIG. 5. High-voltage circuit using bias potentials.

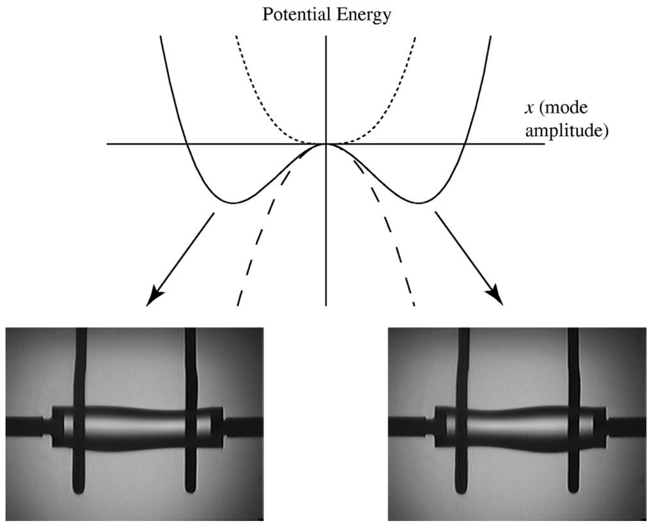

FIG. 6. The dashed curve shows the quadratic dependence of surface free energy with the (2, 0) mode amplitude x, while the dotted curve shows the cubic dependence on x of the potential energy associated with the feedback force. The solid line is the sum of the two, with an unstable equilibrium at $x=0$, and two stable equilibria having $x\neq 0$, as shown by the images of a bridge of $S=3.5$ near each stable equilibrium.

limit. The results of the tests on each of the three methods are described here with a discussion of the relative advantages at the end. Unless noted otherwise, the volume of the bridge is $V=V_{\mathrm{cyl}}=\pi R^2 L$.

A. Method 1: Simple feedback

In this method, when the bridge begins to deform by one end getting thin and the other end rotund, a voltage proportional to the amplitude of the deformation is applied to the electrode near the thin end of the bridge. It was found to be possible to stabilize a bridge to a slenderness value of 4.3 with this method, although it was nearly impossible to maintain a cylindrical shape. As shown in the images of Fig. 6, the static bridge shape was deformed, with one end rotund and the other thin. By changing the offset voltage in the feedback algorithm it was possible to cause the rotund part of the bridge to move to the opposite side but it was very difficult if not impossible to tune the offset voltage in such a way that the bridge was cylindrical. This can be understood by considering the potential energy of the system. For bridges longer than $S=\pi$, the surface free energy contribution of the (2, 0) bridge mode grows negative in proportion to the square of the deformation amplitude. The work done by the electrostatic stress on the bridge as it goes from a cylindrical to a deformed shape is proportional to the cube of the absolute deformation amplitude. The potential energy of the system is then the sum of the surface free energy and the work done by the feedback force which, as shown in Fig. 6, gives a double-well potential. Thus one would expect two stable equilibrium shapes which have mirror-opposite deformations while the cylindrical state is an unstable equilibrium.

B. Method 2: Square-root feedback

The second method tried is similar to the first method in that a voltage is applied to the electrode near the end of the bridge which begins to get thin; however, in this case, the voltage is applied in proportion to the square-root of the deformation amplitude instead of in direct proportion. This overcomes the difficulty experienced with the first method, which gave stable equilibria which were not a cylindrical shape. With the proper feedback gain the potential energy of the system in this case has a single stable equilibrium point corresponding to a cylindrical shape. This is because both the surface free energy and the work done by the electric field are quadratic in the deformation amplitude. The experimental tests of this method confirm that the cylindrical state is stable. Using this method, bridges with near-cylindrical volume could be extended to slenderness values near the theoretical cylindrical-bridge limit $S_3\approx 4.49$. In approaching this limit, the volume of liquid in the bridge became critical to its stability. The bridge deployment system described in Sec. III A was not capable of reproducibly creating bridges of precisely cylindrical volume, with errors of 1%–3% being typical. Accurate measurements of bridge volumes were not made in real time. The equilibrium shapes of bridges with a slenderness near S_3 take on (3, 0) mode characteristics if the volume is slightly greater or less than that of the cylinder. Bridges with just a few percent greater volume than the cylinder have a bulge in the center and could be stabilized even beyond the S_3 limit for the cylinder. A stabilized bridge with a volume 2.8% greater than that of a cylinder and with a slenderness of 4.48 is shown in Fig. 7(a). Bridge volume was measured by integrating πr^2 over the length of the bridge

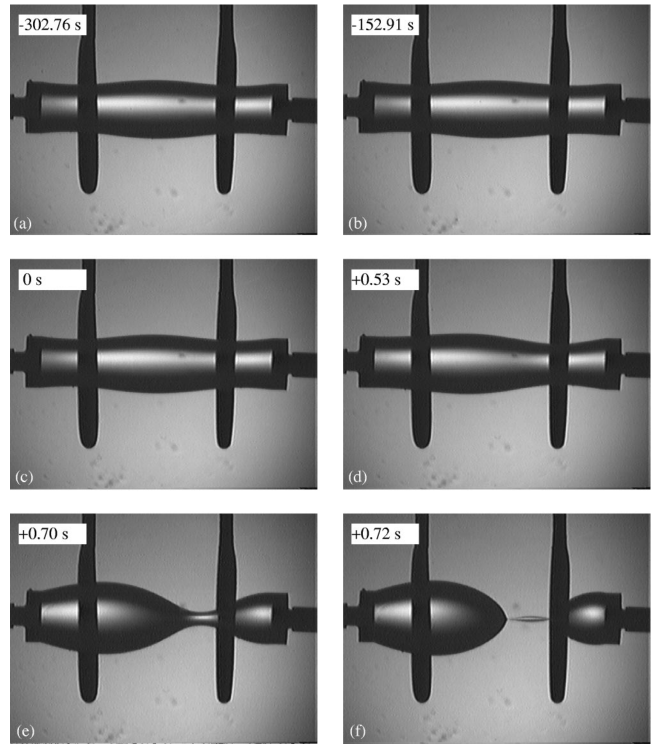

FIG. 7. A time sequence showing a bridge with slenderness 4.48 actively stabilized using the square-root feedback algorithm. Frames (a)–(c) show the bridge being stabilized for about 5 min. In frame (c) the feedback control is turned off. Frames (d) through (f) show the subsequent growth of the (2, 0) mode and bridge breakage which occurs less than a second after control is turned off.

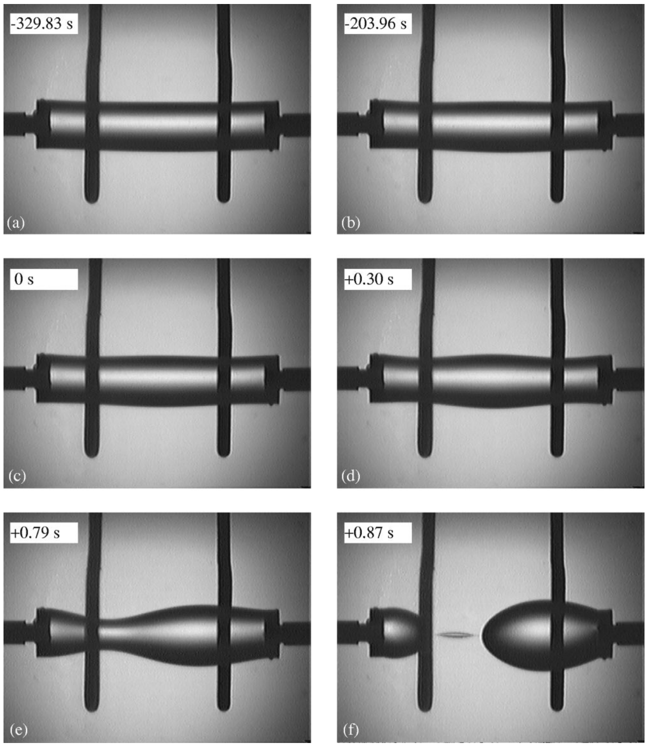

FIG. 8. A time sequence showing a bridge with slenderness 4.4 actively stabilized using the bias-potential method where $V_b = 300$ V. Frames (a)–(c) show the bridge being stabilized for over 5 min. In frame (c) the feedback control is turned off. Frames (d) through (f) show the subsequent growth of the (2, 0) mode and bridge breakage which occurs less than 1 sec after control is turned off.

where the bridge radius profile, $r(z)$, was determined by digital image analysis. The image sequence in Fig. 7 shows a bridge that was stabilized for about 5 min, at which time the feedback control was turned off. Control was turned off at time $t = 0$ s shown in Fig. 7(c), and Figs. 7(d)–(f) show the subsequent growth of the (2, 0) mode and ultimate breakup of the bridge which occurs less than a second after turning off the control.

C. Method 3: Bias potential feedback

Applying a bias voltage to the ring electrodes as described in Sec. II is another way to avoid the problem of a double-well potential experienced with method 1. Figure 8 is a sequence showing a bridge of slenderness 4.4 being stabilized with a bias voltage $V_b = 300$ V. The bridge was stabilized for more than 5 min before the control was turned off. The control and bias voltages are turned off in frame (c) at time $t = 0$ s and frames (d)–(f) show the subsequent growth of the (2, 0) mode and bridge breakage. It is interesting to note that shortly after control was turned off, in frame (d) the bridge relaxes to a near-equilibrium (3, 0) shape such as that seen during active control with the square-root method. This is because the relaxation time of the stable (3, 0) mode is shorter than the growth time of the unstable (2, 0) mode which ultimately leads to breakup. The (3, 0) shape with a bulge in the center seen in Fig. 8(d) indicates that the volume of this bridge was somewhat greater than that of a cylinder. This was confirmed by an independent measurement of bridge volume using digital image analysis which gave a volume 2% greater than that of a cylinder. The bias potential on the ring electrodes is thus seen to make the bridge look more cylindrical even though the volume is greater than the cylindrical volume. On the other hand, when the volume is that of a cylinder, the bias voltage tends to give a static shape which bulges beneath the electrodes and is thin in the center. This leads to pinch off of the bridge in the center before reaching the slenderness limit of S_3.

D. Discussion of results

All three methods of stabilization which were tested proved capable of stabilizing bridges having a volume $\pi R^2 L$ well beyond the Rayleigh–Plateau limit. The simplest feedback method (where the electrode voltages are proportional to the error signal) has the disadvantage that it gives a static (2, 0) shape during stabilization. The ultimate slenderness achieved with this method was significantly less than the theoretical maximum of S_3.

The square-root method has the advantage over the other two methods that it does not affect the static shape of the bridge; this generally makes for a more stable situation. The noncylindrical equilibrium shapes that are seen if the volume is not exactly that of a cylinder are those expected from theory as discussed below.

The main drawback of the bias-potential method is that for a bridge with cylindrical volume, the bias potentials on the rings cause a noncylindrical equilibrium shape which is thin in the center, causing a reduction in stability. On the other hand, for bridges with volumes a few percent greater than cylindrical, the bias potentials on the rings cause the bridge shape to be more cylindrical than it would otherwise be. The problems caused by the bias potential could be reduced by reducing the magnitude of the bias potential; however, the minimum level of bias is dictated by the minimum gain needed for stabilization.

While it was not the emphasis of our observations, it is noteworthy that the conical shapes visible in Figs. 7(f) and 8(f) are reminiscent of shapes associated with jet breakup.[12,13,21]

E. Theoretical bridge equilibria and comparison with observation

The equilibrium shapes seen for stabilized bridges near S_3 can be better understood by looking at the stability diagram in Fig. 9 calculated using the methods of Lowry and Steen.[22–24] In this graph, the stability of bridges is plotted as a function of the normalized bridge volume and slenderness. In the shaded areas, bridges are only unstable to the (2, 0) mode, and in principle may be stabilized by the methods described. In the unshaded region, the (3, 0) mode is also unstable and the bridge will break. This graph is only valid for the square-root feedback method, since the bias potential method introduces additional forces which alter the equilibrium bridge shapes and would be expected to shift stability boundaries.

Representative bridge shapes are shown for each of the stabilized regions. In the small darker-shaded area with V

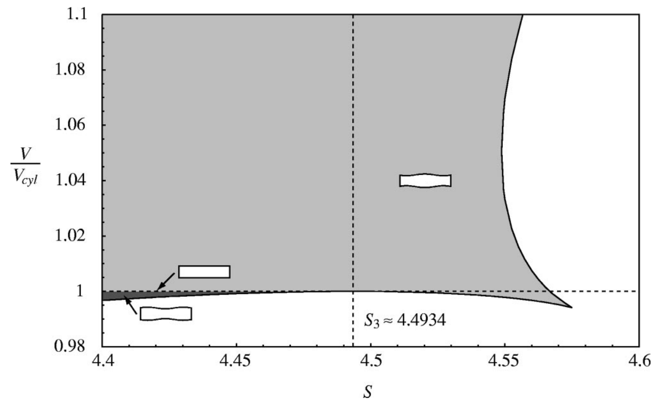

FIG. 9. A stability plot of normalized volume V/V_{cyl} vs slenderness S for near-cylindrical capillary bridges near the critical slenderness $S_3 \approx 4.4934$. In the shaded regions, only the (2, 0) mode is unstable, and the bridge may be stabilized by the method described. In the unshaded region, the (3, 0) mode is unstable, and the stabilized bridge will break.

$<V_{\mathrm{cyl}}$ and $S<S_3$, the shape is rotund at the ends, and thin in the middle. Along the $V=V_{\mathrm{cyl}}$ line for $S<S_3$, the bridge shape is a cylinder. In the lighter-shaded area, the bridge is rotund in the middle, and thin on the ends. Note that on the $V=V_{\mathrm{cyl}}$ line for $S>S_3$ the stabilized shape is not a cylinder, even though the bridge has cylindrical volume.

Near S_3, the slenderness limit is strongly dependent on bridge volume. A deficiency in bridge volume of less than 0.4% from cylindrical causes the maximum slenderness to decrease by 2%, while it is predicted that a slightly overinflated bridge can be stabilized to $S>4.55$.

Comparisons between the theoretical shapes obtained as above and the observed shapes of bridges stabilized using the square-root method are shown in Figs. 10 and 11. The volumes of the bridges for the theoretical shape calculations were chosen to give a good qualitative shape comparison with the experimental images. Independent measurement of the bridge volumes from the corresponding experimental images gave volumes very close to those chosen for the theoretical calculations. The experimentally observed shapes seen in Figs. 10(a) and 11(a) are compared to theoretical shapes which are solutions to the Young–Laplace equation with no external force fields as shown in Figs. 10(b) and 11(b). The theoretical shapes are shown as computer-generated ray-traced images for a qualitative comparison with the experimental images. This comparison suggests that the static shape of the bridge is not influenced by the control system. The control system simply prevents the growth of the lowest-order unstable mode, allowing equilibrium shapes which are normally unstable to be seen. As expected, bridges with volumes less than that of the cylinder are found to be more unstable, tending to pinch off in the center before reaching a slenderness of S_3.

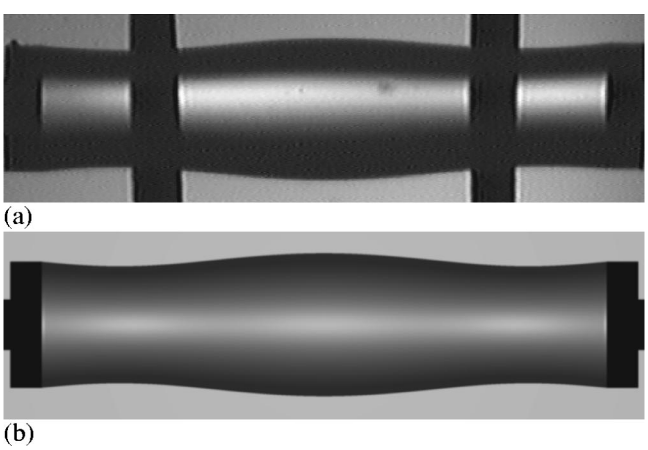

FIG. 10. (a) Photograph of a bridge with $S=4.48$ which is actively stabilized using the square-root algorithm. The volume was measured to be 2.8% greater than that of a cylinder. (b) Computer generated image of a bridge shape calculated from the Young–Laplace equation assuming no external forces. The calculation was performed for a bridge with $S=4.48$ and a volume which is 2.9% greater than that of a cylinder.

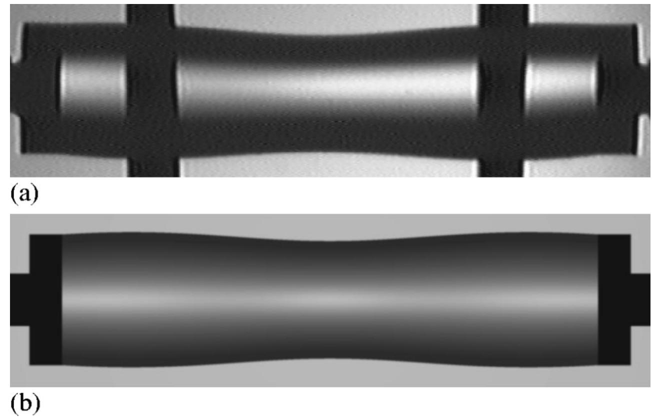

FIG. 11. (a) Photograph of a bridge with $S=4.1$ which is actively stabilized using the square-root algorithm. The volume was measured to be 2.5% less than that of a cylinder. (b) Computer generated image of a bridge shape calculated from the Young–Laplace equation assuming no external forces. The calculation was performed for a bridge with $S=4.1$ and a volume which is 3.2% less than that of a cylinder.

V. RELATED APPLICATIONS

While the research results described concern the active stabilization of the (2, 0) mode of electrically conducting bridges in (simulated) zero gravity, there are related noteworthy applications. With a modified sensor and electrode array, it is plausible that both the (2, 0) and (3, 0) modes could be controlled. The control method described should also be applicable to the suppression of the RP instability of a dielectric liquid layer which coats a grounded conducting cylinder. For the situation in which there are two electrodes, the liquid dielectric will have the greatest attraction to the electrode where the potential has the largest magnitude, as with the electrically conducting bridges studied. For electrically conducting bridges having $S<\pi$, axisymmetric modes of the bridge were excited with an appropriate modulation of the electrode potentials. (That demonstration is analogous to the excitation of modes with modulated acoustic radiation pressure.[9]) Observations (not presented here) also show that it is possible to modify the static profile of a vertical electrically conducting bridge in air with radial electric fields even for non-negligible Bond numbers. For this application, however, the fields required to counteract gravity may be large, as is evident by the following estimate. Consider a vertical conducting bridge surrounded by a gas in an effective gravity of g_e. The magnitude of the hydrostatic pressure differential for a bridge of length L and density ρ is $\rho g_e L$. If a radial field E is applied to the upper portion of the bridge to counteract the bulge of the lower portion of the bridge, the Maxwell stress is radially outward with a magnitude of[25] $(1/2)\epsilon_0 E^2$, where $\epsilon_0 \approx 8.85\times 10^{-12}$ F/m is the permittivity of free space. Though the magnitude of the applied stress required to suppress a bulge of a given size is affected by surface tension, for the purpose of estimating the magnitude of E, take $(1/2)\epsilon_0 E^2 = \rho g_e L$; with $\rho = 1$ g/cm^3, $L = 1$ cm, and a reduced gravity of $g_e = 29$ cm/s$^2 = 30$ mg, this estimate gives $E \approx 8.1\times 10^5$ V/m. The electrode potentials required depend on the electrode dimensions. The gap between the electrode and the bridge may not be small so as to avoid a lateral instability of a liquid column described by Taylor.[26]

ACKNOWLEDGMENT

This work was supported by NASA.

APPENDIX: ELECTRODES AND BRIDGE ELECTRICAL CONDUCTIVITY

The selection of the radius and thickness of the conducting rings used as the electrodes was guided by the following calculation. Consider the electrostatic potential $\phi(z,r)$ for a uniformly distributed ring of charge of radius $a > R$ which is coaxial with an infinitely long grounded conducting cylinder of radius R. The ring lies in the plane $z=0$. The solution for this simplified potential distribution is useful for estimating the field distribution near the bridge under conditions which apply to the actual system under consideration. Some of the simplifications involved include neglecting the perturbation of the field introduced by the second electrode and the requirement that an equipotential surface for the simplified problem closely approximate the surface of the conducting electrode. In addition, the perturbation of the field associated with the wire which supports the electrode (and connects it to the circuits described in Sec. III) is neglected, as are the perturbations resulting from deformation of the bridge. The potential for the simplified geometry is proportional to the Green function

$$\nabla^2 G(\mathbf{r}) = -\frac{4\pi}{r}\,\delta(r-a)\,\delta(z), \tag{A1}$$

where r denotes the radius in cylindrical coordinates. The boundary condition is that $G=0$ at $r=R$ for all z. This is solved using standard potential theory[27] by using a Fourier transform representation for the z dependence of both G and $\delta(z)$, which leads to the following condition on $g(r,k_z)$, the Fourier transform of G:

$$\frac{d}{dr}\left(r\frac{dg}{dr}\right) - rk_z^2 g = -4\pi\,\delta(r-a). \tag{A2}$$

The solution is

$$g(r,k_z) = -4\pi[B(k_z)K_0(k_z r_<) - I_0(k_z r_<)]K_0(k_z r_>), \tag{A3a}$$

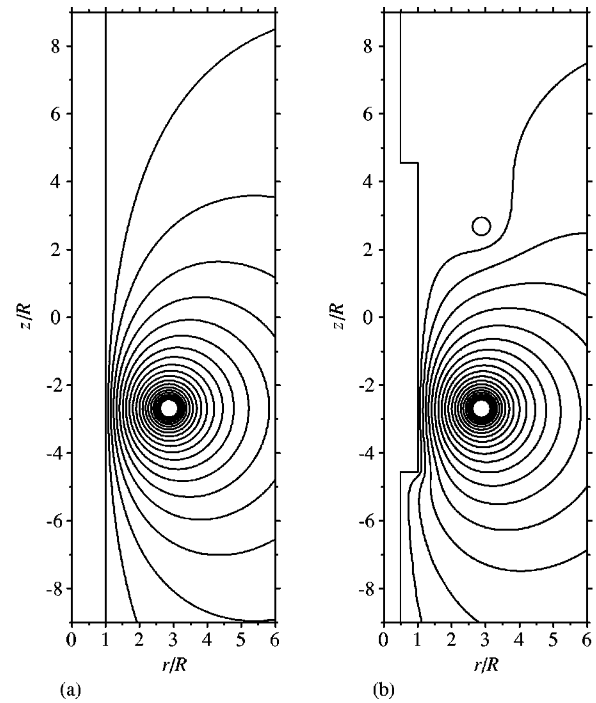

FIG. 12. Equipotential contours of the axisymmetric electric field surrounding the bridge. (a) Analytical result for the simplified geometry of an infinite grounded cylinder and concentric ring of charge. For ease of comparison with (b), the plane of the electrode is offset to $z/R = -2.69$. (b) Finite element result for a more realistic geometry with a bridge of slenderness $S=4.0$ and with the dimensions of the electrodes, support disks, and posts corresponding to the experimental situation. The center of the bridge corresponds to $z=0$.

where $r_>(r_<)$ is the greater (lesser) of r and a, $B(k_z) = I_0(k_z R)/K_0(k_z R)$, and G is given by

$$G(r,z) = \frac{1}{4\pi^2}\int_{-\infty}^{\infty} g(r,k_z)e^{ik_z z}dk_z. \tag{A3b}$$

The electric field at the surface of the circular cylinder is proportional to $-\partial G/\partial r$ evaluated at $r=R$ and is given by

$$E_r(z) = A\int_0^{\infty} k_z \cos k_z z[B(k_z)K_0'(k_z R) - I_0'(k_z R)] \times K_0(k_z a)dk_z, \tag{A4}$$

where A is a constant. The relevance of these results to the electrode configuration used is evident by inspection of Fig. 12(a), which shows equipotential contours for the situation where the radius a of the charged ring is $2.87R$. Inspection of the contours shows them to be nearly circular in the region close to the ring. Consequently, the potential distribution closely approximates that of a conducting torus provided the cross-sectional area of the torus is sufficiently small. The ratio $a/R \approx 2.87$ was selected by evaluating the distribution of the Maxwell stress on the surface of a cylindrical bridge normalized to the peak value (which occurs in the plane of the ring which is at $z=0$). Figure 13 shows this normalized stress $E_r^2(z)/E_r^2(0)$ which from Eq. (A4) may be expressed as

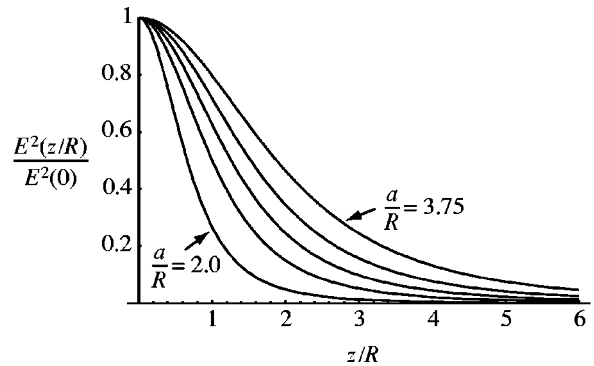

FIG. 13. A plot of the normalized stress distribution for the following normalized ring radii a/R:2.0, 2.5, 2.87, 3.25, and 3.75.

$$\frac{E_r^2(z)}{E_r^2(0)}=\left\{\int_0^\infty \cos\left(\frac{\beta z}{R}\right)\left[\frac{K_0(\beta a/R)}{K_0(\beta)}\right]d\beta\right\}^2 \Big/ \left\{\int_0^\infty \left[\frac{K_0(\beta a/R)}{K_0(\beta)}\right]d\beta\right\}^2, \tag{A5}$$

where $\beta=k_zR$ and the expression $W[K_0(\beta),I_0(\beta)]=1/\beta$ has been used where W denotes the Wronskian. The final result for $E_r(z)$ was confirmed using a finite element method (FEM) to evaluate the potential and the associated field. As the ratio a/R approaches unity, the ratio in Eq. (A5) becomes narrowly peaked around $z=0$ and if a is taken to be much larger than R, the stress distribution is overly broad so that both the left and right sides of the bridge are stressed. To optimize the ''footprint'' of the stress, the following Fourier coefficient was evaluated;

$$C_f=\frac{1}{R}\int_{-\lambda/4}^{3\lambda/4}\cos\left(\frac{2\pi z}{\lambda}\right)\left[\frac{E_r(z)}{E_r(0)}\right]^2 dz, \tag{A6}$$

for $\lambda=2\pi R$ with a range of a/R used in the evaluation of Eq. (A5). This coefficient is a useful measure of the coupling to the (2, 0) mode at the critical wavelength $\lambda=2\pi R$ which naturally becomes unstable when $S=\pi$. This is because $\cos(2\pi z/\lambda)$ approximates the shape of the mode in the limit of infinitesimal deformation.[3] Numerical evaluation shows the Fourier coefficient C_f has a broad maximum centered on $a=2.87R$.

The stress distribution on the bridge predicted by the analytical solution for the simplified geometry described above was checked using a FEM to compute the field for a more realistic geometry. A finite element solution was determined for a geometry which included two wire electrodes, one of which has a nonzero potential and the second being held at ground potential. The electrode dimensions, including wire diameter and ring diameter, and the support-post geometry corresponding to the experimental situation for a bridge of slenderness $S=4.0$, were used in the computation. Figure 12(b) gives the equipotential contours from the FEM computation for the experimental geometry. Figure 12(a) shows the analytical results for the potentials using the same ratio of electrode ring radius to bridge radius. The potentials in Fig. 12(a) were scaled so that the equipotential contour which is positioned approximately at the electrode surface is given the same potential as the electrode potential in Fig. 12(b). The FEM results indicate that the second electrode being held at ground potential shields the part of the bridge beneath it. Aside from this, the stress distribution computed by the two methods is very similar in the region where the stress is large.

While this analysis assumes that the bridge is sufficiently electrically conducting to remain at zero potential, the requirement on the conductivity of the liquid is not very restrictive. The requirement on the conductivity σ_e of the bridge liquid may be estimated as follows. The resistance from the closest end to the adjacent displacement antinode is roughly $R_e\approx L/(\sigma_e 4\pi R^2)$, while the actual resistance will be somewhat lower because of current flow from the support at the opposite side of the bridge. The electrical time constant of the electrode-bridge system may be approximated as $\tau_e=R_eC_e$, where C_e is the electrode capacitance with respect to the bridge. Taking $\tau_e\lesssim\tau$, the time constant in Eq. (5), and $L=2SR$ (where S is the slenderness) gives $\sigma_e \gtrsim SC_e/2\pi R\tau$. For example, typically $C_e\approx 200$ pF, $R\approx 2$ mm, $S=4$, and $\tau\approx 0.1$ ms gives $\sigma_e\gtrsim 10\ \mu$S/cm, whereas the salt solution used had $\sigma_e>20$ mS/cm. For comparison, molten and hot solid silicon have[28] $\sigma_e\gtrsim 10\,000$ S/cm.

[1] J. A. F. Plateau, ''Experimental and theoretical researches on the figures of equilibrium of a liquid mass withdrawn from the action of gravity,'' A. Rep. Board Reg. Smithson. Inst., p. 207 (1863).
[2] Lord Rayleigh, ''On the capillary phenomena of jets,'' Proc. R. Soc. London **29**, 71 (1879).
[3] W. G. Pfann and D. W. Hagelbarger, ''Electromagnetic suspension of a molten zone,'' J. Appl. Phys. **27**, 12 (1956).
[4] B. J. Lowry and P. H. Steen, ''Flow-influenced stabilization of liquid columns,'' J. Colloid Interface Sci. **170**, 38 (1995).
[5] L. A. Slobozhanin, J. I. D. Alexander, and A. H. Resnick, ''Bifurcation of the equilibrium states of a weightless liquid bridge,'' Phys. Fluids **9**, 1893 (1997).
[6] S. Sankaran and D. A. Saville, ''Experiments on the stability of a liquid bridge in an axial electric field,'' Phys. Fluids A **5**, 1081 (1993).
[7] B. J. Lowry and P. H. Steen, ''Stability of slender liquid bridges subjected to axial flows,'' J. Fluid Mech. **330**, 189 (1997).
[8] M. J. Marr-Lyon, D. B. Thiessen, and P. L. Marston, ''Stabilization of a cylindrical capillary bridge far beyond the Rayleigh-Plateau limit using acoustic radiation pressure and active feedback,'' J. Fluid Mech. **351**, 345 (1997).
[9] S. F. Morse, D. B. Thiessen, and P. L. Marston, ''Capillary bridge modes driven with modulated ultrasonic radiation pressure,'' Phys. Fluids **8**, 3 (1996).
[10] A. Eyer, H. Leiste, and R. Nitsche, ''Floating zone growth of silicon under microgravity in a sounding rocket,'' J. Cryst. Growth **71**, 173 (1985).
[11] D. Langbein, ''Crystal growth from liquid columns,'' J. Cryst. Growth **104**, 47 (1990).
[12] D. H. Peregrine, G. Shoker, and A. Symon, ''The bifurcation of liquid bridges,'' J. Fluid Mech. **121**, 25 (1990).
[13] J. Eggers, ''Nonlinear dynamics and breakup of free-surface flows,'' Rev. Mod. Phys. **69**, 865 (1997).
[14] D. Quere, ''Fluid coating on a fiber,'' Annu. Rev. Fluid Mech. **31**, 347 (1999).
[15] M. S. Longuet-Higgins, B. R. Kerman, and K. Lunde, ''The release of air bubbles from an underwater nozzle,'' J. Fluid Mech. **230**, 365 (1991).
[16] T. Surek and S. R. Coriell, ''Shape stability in float zoning of silicon crystals,'' J. Cryst. Growth **37**, 253 (1977).
[17] H. E. Covert, ''Sustainability of small scale floating zones under microgravity,'' Ph.D. dissertation, Massachusetts Institute of Technology, Cambridge, MA, 1998.
[18] A. Sanz, ''The influence of the outer bath in the dynamics of axisymmetric liquid bridges,'' J. Fluid Mech. **156**, 101 (1985).
[19] The estimate $S_3\approx 3\pi/2$ noted in Marr-Lyon *et al.* (Ref. 8) exceeds the

correct value of S_3, although as $n \to \infty$, for odd $n, S_n \to n\pi/2$. See Sanz (Ref. 18) for the correct S_3.

[20]C. R. Fuller, S. J. Elliott, and P. A. Nelson, *Active Control of Vibration* (Academic, San Diego, 1997).

[21]I. Cohen, M. P. Brenner, J. Eggers, and S. R. Nagel, ''Two fluid drop snap-off problem: Experiments and theory,'' Phys. Rev. Lett. **83**, 1147 (1999).

[22]B. J. Lowry and P. H. Steen, ''Capillary surfaces: Stability from families of equilibria with application to the liquid bridge,'' Proc. R. Soc. London, Ser. A **449**, 411 (1995).

[23]B. J. Lowry, ''Shape stability of slender liquid bridges in axial flows,'' Ph.D. dissertation, Cornell University, Ithaca, NY, 1994.

[24]B. J. Lowry, ''The double-helical branch structure of fixed contact line liquid bridge equilibria—stability of long cylindrical liquid bridges,'' Phys. Fluids **12**, 996 (2000).

[25]D. A. Saville, ''Electrohydrodynamics: The Taylor–Melcher leaky dielectric model,'' Annu. Rev. Phys. Chem. **29**, 27 (1997).

[26]G. I. Taylor, ''Electrically driven jets,'' Proc. R. Soc. London, Ser. A **308**, 453 (1969).

[27]J. D. Jackson, *Classical Electrodynamics*, 2nd ed. (Wiley, New York, 1975).

[28]Y. Masuda, T. Tsukada, M. Hozawa, N. Imaishi, and N. Ohnishi, ''Numerical simulation of heat transfer in floating zone crystal growth process with radio-frequency induction heating,'' Int. J. Heat Mass Transf. **39**, 3035 (1996).